Rock Mech Rock Engng (2009) 42: 319–339
DOI 10.1007/s00603-007-0137-8
Printed in The Netherlands

Rock Mechanics and Rock Engineering

Visco-Plastic Behaviour around Advancing Tunnels in Squeezing Rock

By

D. Sterpi and **G. Gioda**

Department of Structural Engineering, Politecnico di Milano,
P. Leonardo da Vinci 32, Milan, Italy

Received July 6, 2006; accepted December 22, 2006
Published online June 12, 2007

Summary

The visco-plastic behaviour of rocks plays a relevant role in the tunnelling works, especially for deep tunnels subjected to large initial stresses for which squeezing conditions may develop. A rheological model is discussed that accounts for visco-elastic (primary) and visco-plastic (secondary) contributions to rock creep. The effects of tertiary creep are included in the model by way of a gradual mechanical damage governed by the cumulated visco-plastic strains. The parameters of the intact rock are first identified based on laboratory test results presented in the literature. Then, after scaling them to those of the rock mass, the potential applicability of the model is tested through axisymmetric and plane strain finite element analyses of the full face excavation of a deep circular tunnel. The results are discussed with particular reference to the short term redistribution of stresses around the opening and to its convergence. The analyses show the relevant influence of tertiary creep on the tunnel closure. In addition, those based on an axisymmetric scheme turn out to be crucial for the correct long term prediction of the interaction between the rock mass and the supporting structure of the opening.

Keywords: Creep, squeezing, rock mass behaviour, deep tunnels, tunnel face, finite element analysis.

1. Introduction

The stress redistribution induced in a rock mass by a tunnel excavation causes the occurrence of deviatoric stresses around the opening. When the rock mass is characterized by a time-dependent mechanical behaviour, these stresses involve time-dependent deviatoric strains that contribute to increase, in the short and long term, the tunnel closure associated with the stress release. Here ''short term'' and ''long term'' refer, respectively, to conditions that develop during the progress of excavation or after its completion, when the permanent support is already installed.

At great depth, where the rock mass is subjected to large initial stresses, the stress redistribution may lead to the so called squeezing conditions (Barla, 1995). These conditions yield non reversible deviatoric creep strains that develop during time at constant and eventually increasing rate, namely the secondary and tertiary creep stages. This behaviour usually characterizes weak or altered rocks and, for very deep excavations, it can be experienced also in hard rocks (Dusseault and Fordham, 1993; Malan, 2002).

The consequences of squeezing consist of large tunnel closures and of high pressures exerted by the rock mass on the heading support, or on the shield of the Tunnel Boring Machine (TBM) in case of mechanized tunnelling. In extreme conditions, the convergence may increase so rapidly (short term effect) that the available thrust for advancing the TBM becomes insufficient and the ground slowly locks the machine (Steiner, 1996; Einstein and Bobet, 1997). Considering the limited gap existing between the TBM shield and the excavated surface these conditions could occur even for a relatively small inward convergence of the rock mass.

In engineering practice, the prediction of the squeezing potential is based on in situ measurements, usually concerning the state of stress and the rock mass strength. For a refined prediction of the rock mass response to excavation, however, a proper description of its visco-plastic behaviour and a proper calibration of the mechanical parameters seem necessary. Considering the differences between the behaviour of the intact rock and that of the rock mass, the calibration of the mechanical parameters would require performing tests directly on the rock mass in situ. This, however, is rarely done for the time dependent effects, basically due to operational difficulties.

The visco-plastic behaviour of rocks has been widely discussed in the literature, on the basis of experimental findings from laboratory or field investigations, constitutive modelling and numerical analyses (e.g. Ladanyi, 1993; Cristescu and Gioda, 1994; Cristescu and Hunsche, 1998; Pellet et al., 2005) and special issues of national and international journals have been entirely devoted to this topic (Rock Mechanics and Rock Engineering, 1996; Rivista Italiana di Geotecnica, 2000).

In this paper, an elasto-visco-plastic rheological model is discussed that accounts for the various components of rock creep (Gioda and Cividini, 1996). The calibration of its parameters is carried out first with reference to the results of laboratory creep tests on intact rock samples presented in the literature. Then, an attempt is made to estimate the same parameters for the in situ rock mass. This step is based on empirical correlations and on a measure of the rock mass conditions. Some comments will point out the intrinsic uncertainties of the method.

The constitutive model has been implemented in a non-commercial finite element code and its potential applicability has been verified considering a circular deep tunnel driven in a homogeneous rock mass subjected to an initial isotropic state of stress. These hypotheses allow for assuming alternatively axisymmetric or plane strain regimes that refer, respectively, to the longitudinal and to the cross sections of the tunnel.

The discussion on the numerical results is focused in particular on the effects of the tunnel face advance on the redistribution of stresses around the opening and on the tunnel closure. From these results some comments are drawn on the contribution of tertiary creep, with reference also to mechanized (TBM) tunnelling, and on the limits of the plane strain scheme in the evaluation of the short term effects.

2. Rheological Constitutive Model

When a sample of weak rock is subjected to deviatoric constant stresses, time dependent deviatoric strains may show up even at low stress levels (Fig. 1). For stresses below a given threshold, the associated strains are fully reversible and transient, i.e. they increase with decreasing rate till a stable value is attained (primary creep or visco-elasticity, Fig. 1a). For a stress level that overcomes the threshold, the deviatoric strains assume an irreversible nature (visco-plasticity, Fig. 1b) and increase at first with constant rate and eventually with increasing rate, giving rise to respectively secondary and tertiary creep. The tertiary creep is responsible for the delayed failure of the sample.

Assuming an isotropic material behaviour, the basic elasto-plastic constitutive model consists of an elastic element for the reversible, deviatoric and volumetric responses (Hooke's tangential G^{el} and bulk B^{el} moduli) and of a plastic slider (De Saint Venant element) characterized by a suitable yield condition $F(\sigma) = 0$. In a comprehensive model for creep behaviour two components should be added accounting for the reversible and irreversible time-dependent responses (cf. Fig. 2).

The visco-elastic element consists of a deviatoric dashpot and a deviatoric elastic substance, both connected with a slider that imposes the limit beyond which primary creep occurs. The slider is characterized by the yield function $F^{ve}(\sigma) = 0$ and carries the geostatic stress, preventing the rock mass from undergoing creep strains due to the deviatoric component of the stress state at rest.

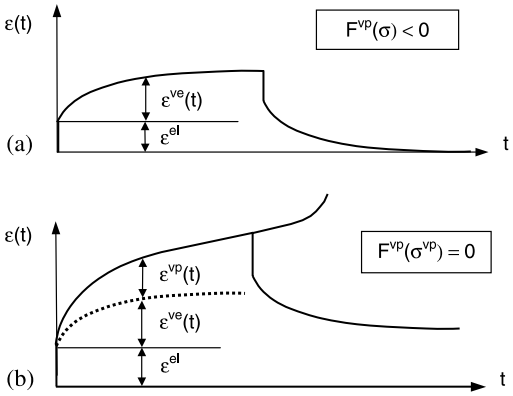

Fig. 1. Creep strain associated with a constant deviatoric stress in loading and unloading paths: (a) primary creep, (b) secondary and tertiary creep

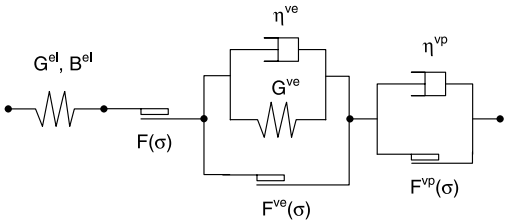

Fig. 2. Rheological model accounting for elastic, plastic, visco-elastic and visco-plastic constitutive behaviour and associated parameters

Besides the yield function F^{ve}, the visco-elasticity is characterized by only two deviatoric parameters: the viscosity coefficient η^{ve} and the tangential modulus G^{ve}. It is reasonable, in fact, to neglect the volumetric creep behaviour of the rock mass.

Under constant stresses the visco-elastic strains increase during time with a decreasing rate, thus leading to an asymptotic value of strains that depends on the value of G^{ve}. The viscosity coefficient governs the decay of the visco-elastic strain rate.

The visco-plastic element (again neglecting the volumetric creep of rock) is the connection of a viscous substance, that carries only deviatoric stress and is characterized by the viscosity coefficient η^{vp}, with a plastic slider, introducing the visco-plastic limit envelope $F^{vp}(\sigma) = 0$. A constant stress exceeding the threshold $F^{vp}(\sigma)$ induces secondary creep, as long as the parameters are constant. The strain rate depends on the value of the viscosity coefficient η^{vp} and on the portion of deviatoric stress carried by the dashpot. If a loss of viscosity η^{vp}, or a reduction of the stress threshold $F^{vp}(\sigma) = 0$, with increasing strains are accounted for, the plastic strain rate increases and leads to tertiary creep and to the eventual failure. The variation of these mechanical characteristics, between maximum (or peak) and minimum (or residual) values, is governed by the cumulated visco-plastic strains in a fashion similar to what, in plasticity, is referred to as strain softening.

Even in the simplest case of isotropic behaviour this constitutive model is characterized by an exceedingly large number of parameters and, hence, is unpractical for applications. To overcome this substantial drawback, a simpler model has been proposed in (Gioda and Cividini, 1996), neglecting the time-independent (or instantaneous) failure governed by the yield condition $F(\sigma)$ and the visco-elastic stress threshold $F^{ve}(\sigma)$ (Fig. 3a). The first assumption requires that the material yielding condition $F(\sigma)$ is substantially larger than the visco-plastic limit $F^{vp}(\sigma)$, whilst the second one confines this model to isotropic distributions of in situ stresses.

Neglecting tertiary creep, the set of mechanical parameters to be identified for the simplified model is shown in Fig. 3a. Here, a Mohr-Coulomb type surface is adopted for the visco-plastic yield condition, with a non-associated flow rule, characterized by cohesion, friction angle and dilatancy parameters. To account for tertiary creep it is necessary to provide a law governing the reduction of these parameters from their peak to their residual values. A piecewise linear law is adopted in the present context (cf. Fig. 3b) expressing the above variation as a function of the square root of the

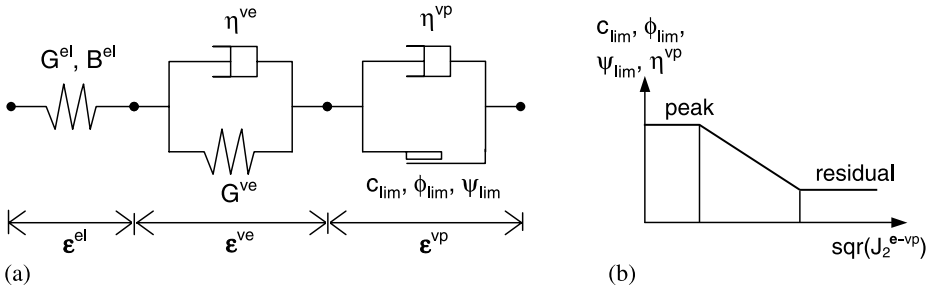

Fig. 3. Simplified rheological model with associated parameters (a) and variation of the visco-plastic parameters with the 2nd invariant of deviatoric visco-plastic strains (b)

second invariant of the deviatoric plastic strains. This, in addition to the peak and residual mechanical parameters, introduces the limit values of the visco-plastic strains associated with the onset of softening and with its completion.

The constitutive equations in matrix form can be worked out as follows. An additive decomposition of the vector collecting the six independent components of the total strain vector is here considered,

$$\boldsymbol{\varepsilon} = \boldsymbol{\varepsilon}^{\mathrm{el}} + \boldsymbol{\varepsilon}^{\mathrm{ve}} + \boldsymbol{\varepsilon}^{\mathrm{vp}}, \tag{1}$$

introducing the elastic $\boldsymbol{\varepsilon}^{\mathrm{el}}$, visco-elastic $\boldsymbol{\varepsilon}^{\mathrm{ve}}$ and visco-plastic $\boldsymbol{\varepsilon}^{\mathrm{vp}}$ contributions to the total strain. These depend on the constitutive relations characterizing each element of the rheological model in Fig. 3. In the isotropic case it is convenient to express these relations through volumetric and deviatoric components of stress and strain,

$$\boldsymbol{\sigma} = \sigma_{\mathrm{m}}\mathbf{m} + \mathbf{s}, \tag{2a}$$

$$\boldsymbol{\varepsilon} = \frac{\varepsilon_{\mathrm{v}}}{3}\mathbf{m} + \mathbf{e}. \tag{2b}$$

In Eqs. (2), σ_{m} is the hydrostatic stress, ε_{v} is the corresponding volumetric strain, $\mathbf{s}$ and $\mathbf{e}$ are the deviatoric stress and strain vectors and the entries of vector $\mathbf{m}$ are equal to 1 or 0 if they correspond, respectively, to normal or shear stresses. The three elements of the rheological model are described by the constitutive relations:

$$\boldsymbol{\sigma} = \mathrm{B}^{\mathrm{el}} \cdot \varepsilon_{\mathrm{v}}^{\mathrm{el}} \cdot \mathbf{I} + 2\mathrm{G}^{\mathrm{el}} \cdot \mathbf{e}^{\mathrm{el}}, \tag{3a}$$

$$\mathbf{s} = 2\mathrm{G}^{\mathrm{ve}} \cdot \mathbf{e}^{\mathrm{ve}} + \eta^{\mathrm{ve}} \cdot \dot{\mathbf{e}}^{\mathrm{ve}}, \tag{3b}$$

$$\mathbf{s}^{\mathrm{vp}} = \eta^{\mathrm{vp}} \cdot \dot{\mathbf{e}}^{\mathrm{vp}}, \tag{3c}$$

where a superposed dot means time derivative and $\mathbf{s}^{\mathrm{vp}}$ is the portion of the deviatoric stress carried by the visco-plastic dashpot. This can be determined by introducing the total stress carried by the plastic slider $\boldsymbol{\sigma}^{\mathrm{vp}}$, which includes the entire hydrostatic stress and fulfils the visco-plastic limit condition,

$$\mathbf{s}^{\mathrm{vp}} = \boldsymbol{\sigma} - \boldsymbol{\sigma}^{\mathrm{vp}}, \tag{4a}$$

$$\sigma_{\mathrm{m}}^{\mathrm{vp}} = \sigma_{\mathrm{m}}, \tag{4b}$$

$$\mathrm{F}^{\mathrm{vp}}(\boldsymbol{\sigma}^{\mathrm{vp}}) = 0. \tag{4c}$$

In addition, the plastic flow rule requires sthat:

$$\dot{\boldsymbol{\varepsilon}}^{\mathrm{vp}} = \dot{\lambda} \cdot \left.\frac{\partial \mathrm{Q}}{\partial \boldsymbol{\sigma}}\right|_{\boldsymbol{\sigma}^{\mathrm{vp}}}, \tag{5}$$

where $\mathrm{Q}(\boldsymbol{\sigma})$ is the plastic potential function and $\dot{\lambda}$ the plastic multiplier rate. An expression for $\dot{\lambda}$ is readily worked out by substituting Eq. (5) into the Eq. (2b) written in terms of visco-plastic strain rates:

$$\dot{\lambda} \cdot \left.\frac{\partial \mathrm{Q}}{\partial \boldsymbol{\sigma}}\right|_{\boldsymbol{\sigma}^{\mathrm{vp}}} = \frac{\dot{\varepsilon}_{\mathrm{v}}^{\mathrm{vp}}}{3}\mathbf{m} + \dot{\mathbf{e}}^{\mathrm{vp}}. \tag{6}$$

and multiplying each side of Eq. (6) by the transpose of vector $\dot{\mathbf{e}}^{vp}$:

$$\dot{\lambda} = \frac{\left(\dot{\mathbf{e}}^{vp}\right)^{T} \cdot \dot{\mathbf{e}}^{vp}}{\left(\dot{\mathbf{e}}^{vp}\right)^{T} \cdot \frac{\partial Q}{\partial \boldsymbol{\sigma}}\Big|_{\boldsymbol{\sigma}^{vp}}}. \tag{7}$$

The finite element formulation of the elasto-visco-plastic problem and the iterative scheme for the time integration procedure is described in detail by Gioda and Cividini (1996).

3. Parameter Identification Based on Laboratory Tests of Intact Rock

In the case of axisymmetric state of stress, the set of governing equations for primary and secondary creep assumes a simple analytical form. Therefore, the mechanical parameters can be calibrated on the basis of laboratory tests, such as uniaxial creep tests or creep tests under constant confining pressure (in the following referred to as biaxial tests), provided that they are carried out at various stress levels in order to activate the various levels of creep.

The time independent response of the sample, subjected to axial compression σ_1 with constant confining pressure, is used for the calibration of Hooke's parameters in Fig. 3a:

$$\varepsilon_1^{el} = \frac{\sigma_1}{3}\left(\frac{1}{3B^{el}} + \frac{1}{G^{el}}\right), \tag{8a}$$

$$\varepsilon_2^{el} = \frac{\sigma_1}{3}\left(\frac{1}{3B^{el}} - \frac{1}{2G^{el}}\right). \tag{8b}$$

For a low deviatoric stress, in addition to the elastic component only visco-elastic deviatoric strains develop, which depend on the applied stress through the well known equation of Kelvin model,

$$\varepsilon_1^{ve}(t) = e_1^{ve}(t) = \frac{\sigma_1}{3G^{ve}}[1 - \exp(-G^{ve}t/\eta^{ve})]. \tag{9}$$

The implicit assumption is made that the visco-elastic volumetric strains are negligible. Consequently, B^{ve} is very large compared to G^{ve} or the visco-elastic Poisson's ratio tends to 0.5.

To evaluate the visco-elastic parameters consider that for long time spans the dashpot is completely relaxed and the strains reach the value associated with G^{ve}, whilst at the test beginning the strain rate depends on the viscosity η^{ve} (cf. Fig. 1a). Hence, from Eq. (9),

$$\varepsilon_{1(t\to\infty)}^{ve} \to \frac{\sigma_1}{3G^{ve}}, \tag{10a}$$

$$\dot{\varepsilon}_{1(t=0)}^{ve} = \frac{\sigma_1}{3\eta^{ve}}. \tag{10b}$$

The parameters ϕ_{lim} and c_{lim} that define the visco-plastic envelope of Mohr-Coulomb type (Eq. 4c),

$$\sigma_1^{vp} = \sigma_2^{vp}\frac{1 + \sin\phi_{lim}}{1 - \sin\phi_{lim}} + \frac{2c_{lim}\cos\phi_{lim}}{1 - \sin\phi_{lim}}, \tag{11}$$

are identified once the stress threshold $\boldsymbol{\sigma}^{vp}$ beyond which secondary creep develops is experimentally determined. Uniaxial tests are not sufficient to this purpose and a series of biaxial tests should be carried out. Note that the parameters ϕ_{lim} and c_{lim} are not associated with the instantaneous failure of the material, which is characterized by values of friction angle and cohesion larger than ϕ_{lim} and c_{lim}.

The visco-plastic strains that arise when the applied stress exceeds the visco-plastic limit condition are governed by: (i) the constitutive Eq. (3c) that depends on the viscosity coefficient η^{vp} and on the exceeding portion of stress $\mathbf{s}^{vp}$, which in turn depends on ϕ_{lim} and c_{lim} (Eqs. 4); (ii) the flow rule (Eq. 5) that depends on the dilatancy angle ψ_{lim} defining the visco-plastic potential function.

The constant rate portion of the visco-plastic strain-time curve can be used to calibrate the viscosity coefficient and the dilatancy angle on the basis of the following expressions (cf. Appendix A):

$$\dot{\varepsilon}_1^{vp} = \frac{3(1 - \sin\psi_{lim})}{2\eta^{vp}(3 - \sin\phi_{lim})}[\sigma_1(1 - \sin\phi_{lim}) - \sigma_2(1 + \sin\phi_{lim}) - 2c_{lim}\cos\phi_{lim}], \tag{12a}$$

$$\dot{\varepsilon}_2^{vp} = -\frac{3(1 + \sin\psi_{lim})}{2\eta^{vp}(3 - \sin\phi_{lim})}[\sigma_1(1 - \sin\phi_{lim}) - \sigma_2(1 + \sin\phi_{lim}) - 2c_{lim}\cos\phi_{lim}]. \tag{12b}$$

As previously mentioned, tertiary creep involves additional parameters that cannot be expressed in analytical form. Therefore, their calibration is performed by a numerical back analysis, which provides an acceptable matching between experimental and numerical results.

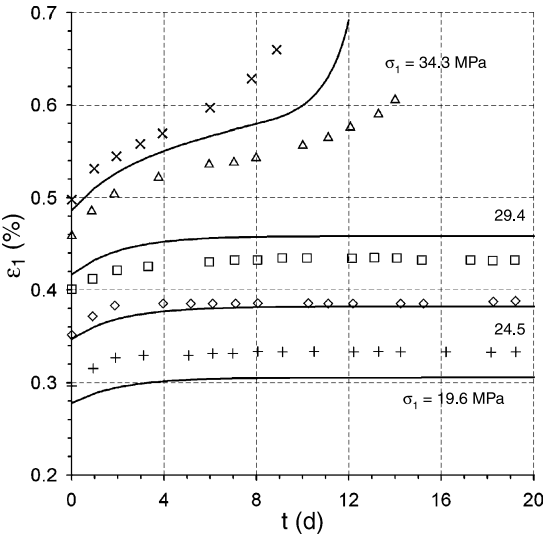

Fig. 4. Uniaxial creep tests on schist: experimental data (dots) (Cristescu and Hunsche, 1998) and numerical results (solid lines)

An example of model calibration is shown in the following with reference to the results of a series of creep tests on schist presented in (Cristescu and Hunsche, 1998). In this process the anisotropy of schist (Kolymbas et al., 2006) has not been investigated. The dots in Fig. 4 represent the variation of axial strain with time for 5 uniaxial compression tests carried out at different load levels constant with time. The two tests carried under the largest stress level, that yielded quite different results, were replaced in the numerical back analysis by a single curve averaging them.

Even though the results of biaxial tests are not available, the shear strength parameters c and ϕ of the instantaneous yield criterion can be evaluated considering that the instantaneous unconfined compression strength of the rock samples is about $\sigma_c = 54$ MPa. This permits defining the Hoek-Brown failure criterion for the intact rock (i.e. for a Rock Mass Rating RMR equal to 100). The corresponding parameters of Mohr-Coulomb condition are then evaluated by matching the two failure criteria (Hoek, 1990; Hoek and Brown, 1997), thus obtaining $c = 13.3$ MPa, $\phi = 37.6°$. Note that Hoek-Brown envelope, here considered with reference to the formulation discussed in (Hoek and Brown, 1988), will be also adopted in Sect. 4 to characterize the rock mass behaviour.

From the experimental data (cf. Fig. 4) the uniaxial stress σ_{lim} that activates visco-plasticity was estimated equal to 32 MPa. This approximately corresponds to a ratio $R_{CS} = 0.6$ between σ_{lim} and σ_c.

To evaluate the parameters c_{lim} and ϕ_{lim} corresponding to σ_{lim} an additional hypothesis is necessary due to the lack of biaxial creep tests. Assuming that the difference between the thresholds of instantaneous failure and of visco-plasticity is due only to a difference in the cohesive contribution, the ratio R_{CS} is applied also to cohesion ($c_{lim} = R_{CS} \cdot c$), while the friction angle remains unchanged ($\phi_{lim} = \phi$).

Table 1. Mechanical parameters referred to the intact rock, from the experimental results of Fig. 4, and to the in situ rock mass, for the deep tunnel problem

	Elastic and visco-elastic parameters			
	B^{el} (MPa)	G^{el} (MPa)	η^{ve} (MPa · d)	G^{ve} (MPa)
Intact rock	5880	2714	49470	23390
Rock mass	1470	678	49470	5848
	Visco-plastic parameters			
	η^{vp} (MPa · d)	c_{lim} (MPa)	ϕ_{lim} (°)	ψ_{lim} (°)
Peak values				
Intact rock	4800	7.88	37.6	20
Rock mass	706	1.16	32.3	14
Residual values				
Intact rock	2400	0	20	0
Rock mass	353	0	20	0

In the paper, the subscript 's' is added to the parameters when referred to the in situ rock mass behaviour.

The above assumptions were introduced solely because of the limited available data. An accurate experimental investigation would in fact permit verifying their correctness and getting an insight into the influence of the rock nature, of the confinement stress, etc. on the time dependent mechanical behaviour.

The values of the intact rock parameters eventually reached are listed in Table 1. Figure 4 shows a comparison between the experimental data (dots) and the numerical results (solid lines) based on the above values.

Note that the visco-elastic strain is relatively small, about 8 and 12% of the purely elastic strains. As a consequence, the shear modulus G^{ve} of the visco-elastic element is appreciably higher than that of the elastic spring G^{el}.

Besides some discrepancies in the initial ($t = 0$) elastic strain, the numerical model apparently provides a reasonable approximation of the test results for both visco-elastic and visco-plastic ranges, including the tertiary creep phase.

4. Parameter Identification for the Rock Mass

The operational difficulties in performing in situ creep tests restrict the direct identification of the rock mass creep parameters to few particular cases. For instance, if relevant squeezing conditions are met during tunnelling, convergence and stress measurements could provide data for the back-analysis of the creep phenomenon (e.g. Dalgiç, 2002; Shalabi, 2005).

In other cases, e.g. involving radioactive waste disposals (Thury and Bossart, 1999), a preliminary full scale tunnel test allows for a direct investigation on rock mass creep (Boidy et al., 2002).

In most cases, however, when results of specific tests are not available, the squeezing potential is empirically evaluated on the basis of index properties related to the quality of the rock mass and to the overburden pressure at the tunnel level (e.g. Aydan et al., 1996; Singh et al., 1997; Hoek, 2001; Barla, 2002).

Another possible approach is frequently adopted in tunnel engineering for assessing the stiffness and shear strength characteristics of the rock mass. It consists in relating them to those of intact samples tested in laboratory through a measure of the conditions of the rock mass in situ. The engineering practice has proved that these scaling rules are effective, although some uncertainty still affects the empirical relationships between laboratory and in situ parameters. This procedure is here extended to the evaluation of the mechanical parameters of the described rheological model.

Let us assume that the Rock Quality Designation (RQD) for the rock mass is equal to 70 and the Rock Mass Rating (RMR) is 48.

The interpretation of a large amount of field data (Hendron, 1968) suggests a reduction factor of 0.25 from laboratory elastic moduli to the field ones when the RQD is equal to 70. Note that other empirical relations could be considered to this purpose (e.g. Serafim and Pereira, 1983; Barton, 2002) that lead to certain scatter of this factor. A recent approach (Hoek and Diederichs, 2006) suggests relating the rock mass stiffness to the Geological Strength Index and to a measure of the rock damage. According to this approach a reduction factor of 0.27 characterizes a relatively undisturbed rock mass, such as the one surrounding a deep tunnel driven with a TBM.

The same reduction can be considered for the shear modulus G^{ve} of the visco-elastic model. In addition, although very few experimental data have been reported in the literature, the visco-elastic strains seem to develop in situ at a rate comparable or even lower than that measured in laboratory (Starfield and McClain, 1973; Chin and Rogers, 1987). As a consequence, the viscosity coefficient η^{ve} could remain unchanged.

Hoek-Brown criterion assigns to this kind of rock mass, with RMR = 48, an unconfined compression strength $\sigma_{c\text{-}s} = 7$ MPa. Then, following the steps already outlined in the previous Section for the intact rock, Mohr-Coulomb parameters for the rock mass are: $c_s = 1.93$ MPa, $\phi_s = 32.3°$.

Lacking specific information, the ratio $R_{CS} = 0.6$ of the intact rock is extended also to the rock mass. Consequently, the uniaxial compression stress that activates the in situ visco-plasticity is $\sigma_{lim.s} = 4.2$ MPa and the parameters of the visco-plastic limit for the rock mass are: $c_{lim\text{-}s} = R_{CS} \cdot c_s$, and $\phi_{lim\text{-}s} = \phi_s$.

Figure 5 summarizes the instantaneous and visco-plastic peak envelopes for intact and in situ rock. The peak dilatancy angle, governing the plastic volume increase due to shear, was assumed equal to 20° for the intact rock and 14° for the rock mass, whilst it vanishes approaching the residual state.

As to the viscosity coefficient of the visco-plastic model, it should be considered that probably η_s^{vp} depends on the same physical causes governing $c_{lim\text{-}s}$. This suggests adopting for η_s^{vp} the same reduction factor already introduced for cohesion.

Finally, the residual state of the rock mass can be assimilated to that of the laboratory samples. Hence the same values were adopted for the two sets of parameters but, as previously mentioned, for the visco-plastic coefficient η_s^{vp}.

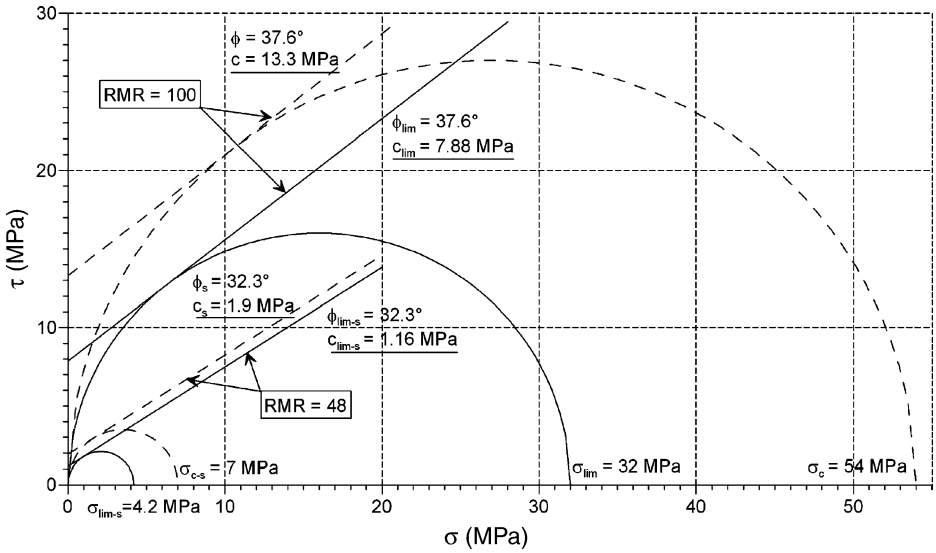

Fig. 5. Mohr-Coulomb yield functions (dashed lines) and visco-plastic functions (solid lines) for intact rock (RMR = 100) and rock mass (RMR = 48)

5. Application to a Tunnelling Problem

The excavation process of a deep tunnel has been analysed by means of the finite element method with the purpose, from the one hand, to get an insight into the effects of squeezing around a deep opening and, from the other hand, to verify the potential applicability of the rheological model in Fig. 3. Some results are discussed in the following with particular reference to the influence of the excavation advance on the convergence and on the stress redistribution around the opening, which is likely to play a major role in mechanized (TBM) tunnelling.

The problem concerns the full face excavation, at a rate of 6 m/day, of a circular tunnel of radius $R = 4.5$ m, in a homogeneous, isotropic rock mass, subjected to an isotropic state of stress $\sigma_0 = 10$ MPa. This corresponds to a tunnel depth of approximately 400 m. The condition of isotropic stress allows neglecting the slider of the visco-elastic component, included in the more comprehensive rheological model of Fig. 2.

5.1 Two-dimensional Axisymmetric Analyses

A first series of 2-dimensional analyses has been carried out in axisymmetric conditions, with reference to the tunnel longitudinal section. The advancing process is explicitly modelled by gradually removing, at a suitable rate, the elements representing the excavated portion of the medium. Besides the limiting assumption of axisymmetric regime, this analysis allows for the direct evaluation of the face effects with an accuracy that depends only on the refinement of the finite element grid along the tunnel axis. The grid consists of 2100 4 node, quadrilateral isoparametric elements and of 2256 nodes, for a total length of 140 m.

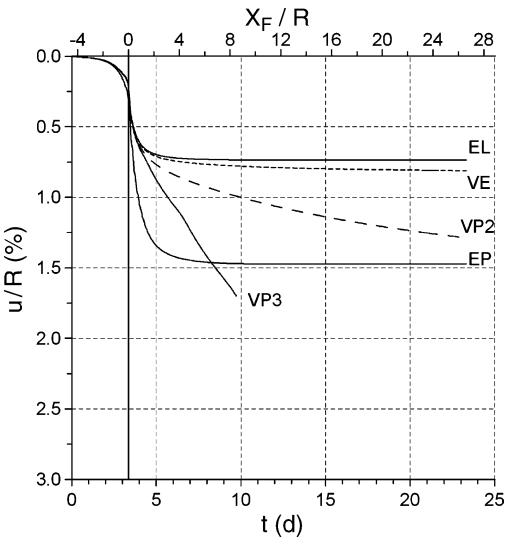

Fig. 6. Tunnel closure with time and with distance X_F from the tunnel face, for various axisymmetric analyses (R = tunnel radius)

The results presented in the following refer to a tunnel section located 20 m apart from the grid border. This section is reached by the tunnel face at a time $t = 3.3$ days after the beginning of excavation. The reason for this choice is two fold. From the one hand, it limits the boundary effects at the chosen section and, from the other hand, allows for a sufficient excavation length (and time) behind the face to observe the full development of visco-plastic effects.

Figure 6 shows the non-dimensional tunnel closure obtained from the following analyses: (VE) visco-elastic analysis; (VP2) visco-plastic analysis limited to secondary creep and based on the peak values of the parameters; (VP3) visco-plastic analysis accounting also for tertiary creep. As a term of comparison, the results have been added of the elastic (EL) and elasto-perfectly plastic (EP) analyses assuming, in the latter case, the parameters c_{lim} and ϕ_{lim} (cf. Table 1) for the rock mass.

The negligible difference between elastic (EL) and visco-elastic (VE) solutions depends on the large value of G_s^{ve} compared to G_s^{el}.

Apparently the maximum tunnel closure u obtained from these analyses (ratio u/R of about 1.5%) should not involve major squeezing problems. However, one should consider that this corresponds to a radial convergence of about 7 cm, which could be larger than the gap existing between the TBM and the perimeter of excavation. If the rate of advancing of the TBM temporarily decreases for some reasons, the convergence would be restrained by a pressure increase on the shield that could gradually lock the machine.

For constant values of the visco-plastic parameters (VP2) the elasto-plastic solution is retrieved in the long term. This result correctly shows that the viscous substance of the visco-plastic element induces only a delay in time of the elasto-plastic solution (EP). Note that a stable convergence is reached in these cases, i.e. the rate of tunnel closure tends to vanish with time.

The results are markedly different in the case of tertiary creep (VP3). In principle, a stable condition is reached also in this case, depending on the residual parameters, but at a much higher value of convergence that would appreciably increase the possible problems for the TBM advancing.

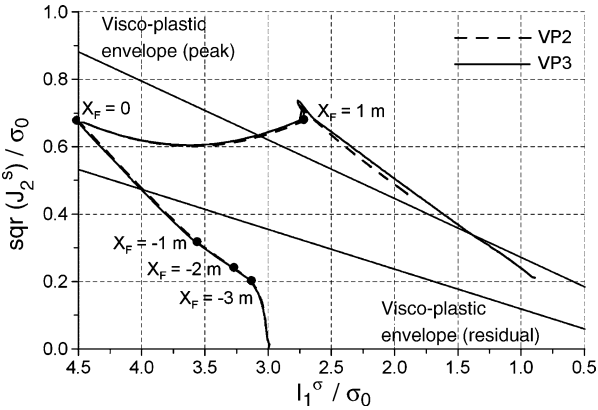

Fig. 7. Stress invariant path at the integration point closest to the tunnel crown for axisymmetric analyses with secondary (VP2) and tertiary (VP3) creep (I_1^σ = 1st invariant of the stress tensor, J_2^s = 2nd invariant of the deviatoric stress tensor, X_F = distance from the tunnel face)

The stress invariant path (Fig. 7) for a point of the rock mass close to the tunnel contour shows that tertiary creep has a minor effect on the evolution of invariants, whilst it appreciably influences the convergence (cf. Fig. 6). In Fig. 7 X_F represents the distance between the advancing excavation face and the point where the stresses are evaluated.

The large increase in the isotropic stress during the face advance reaches its maximum when the tunnel face coincides with the section at hand ($X_F = 0$ in Fig. 7). This depends on the increase of the circumferential and longitudinal stresses (Fig. 8) and, because of friction, yields a temporary increase of resistance in the vicinity of the tunnel face. Note also (Fig. 7) that tertiary creep has an appreciable

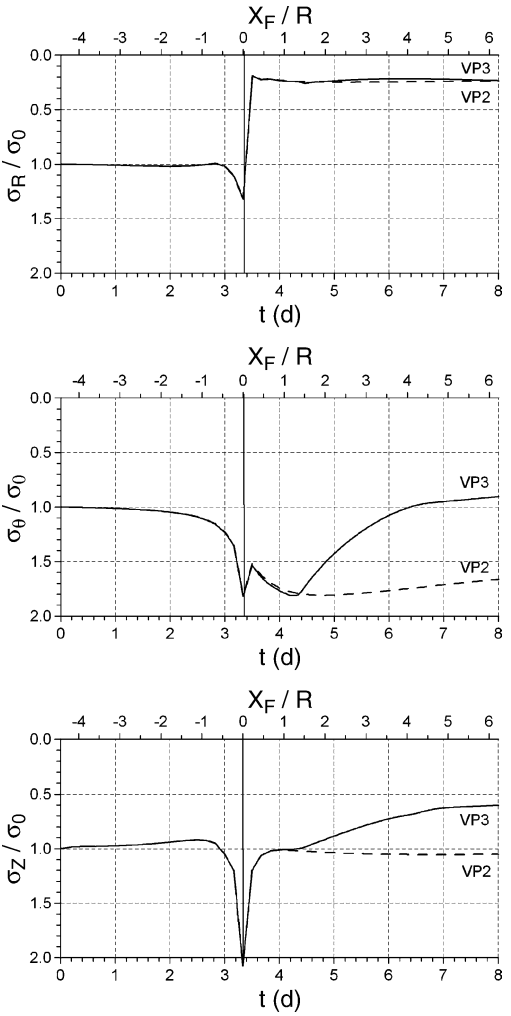

Fig. 8. Variation of principal radial σ_R, circumferential σ_θ and longitudinal σ_Z stresses with time and with distance X_F from the tunnel face, at the integration point closest to the tunnel crown, for axisymmetric analyses with secondary (VP2) and tertiary (VP3) creep (R = tunnel radius)

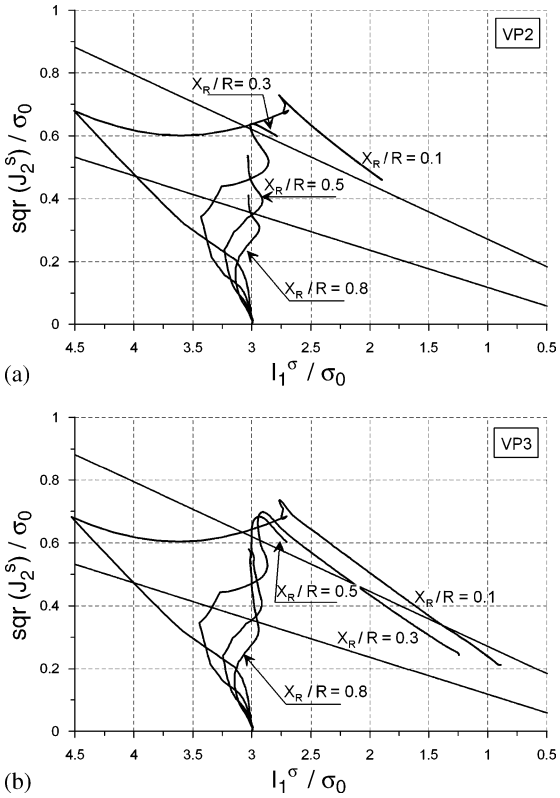

Fig. 9. Stress invariant paths at points at increasing distance X_R from the tunnel crown in the radial direction, for axisymmetric analyses with secondary (a) and tertiary (b) creep (I_1^σ = 1st invariant of the stress tensor, J_2^s = 2nd invariant of the deviatoric stress tensor, R = tunnel radius)

influence on the circumferential σ_θ and longitudinal σ_z stresses, while it marginally affects the radial stress σ_R.

The increase of the isotropic stress tends to vanish with increasing distance from the tunnel contour, as shown in Fig. 9a and b for the VP2 and VP3 analyses, where the same path of Fig. 7 is reproduced for points at increasing distance X_R from the tunnel contour.

5.2 Two-dimensional Plane Strain Analyses

The same problem has been analysed also in a 2-dimensional plane strain regime with reference to the tunnel cross section. In fact this scheme, based on the so called convergence-confinement method (Panet et al., 2001), is frequently adopted in tunnel design particularly to account for the elastic plastic behaviour of rock. However, some limits have been observed when the interest is focused on the effects that the excavation advancing has in the vicinity of the tunnel face (Kielbassa and Duddeck, 1991; Eberhardt, 2001).

In the plane strain scheme the excavation process is modelled through the gradual reduction of ground pressure on the excavated boundary. In elastic plastic ap-

plications this reduction is generally applied at a constant rate. This, however, represents a first drawback in the time dependent case. In fact, the previous analyses show that the effects of the tunnel advance are non-linearly related to the distance of the face from a given tunnel section. This non-linearity has its direct consequence in the non-linear development of the tunnel closure with time, even for a constant advancing rate.

Another drawback of this scheme for creep analyses concerns the choice of the constant rate of reduction of the ground pressure on the tunnel boundary.

A possible way to evaluate the plane strain advancing rate is to relate it to the actual rate of excavation and to the length, along the tunnel axis, of the zone influ-

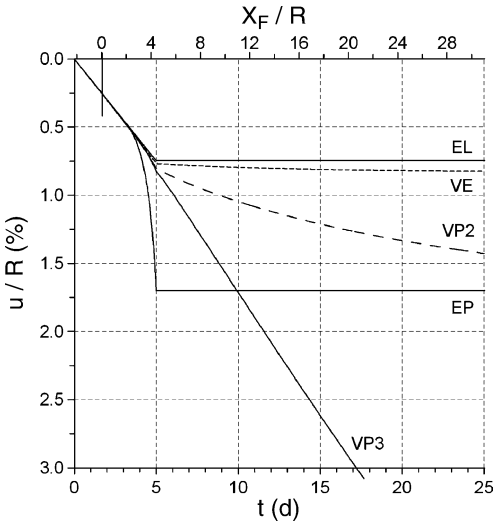

Fig. 10. Tunnel closure with time and with distance X_F from the tunnel face, for various plane strain analyses (R = tunnel radius)

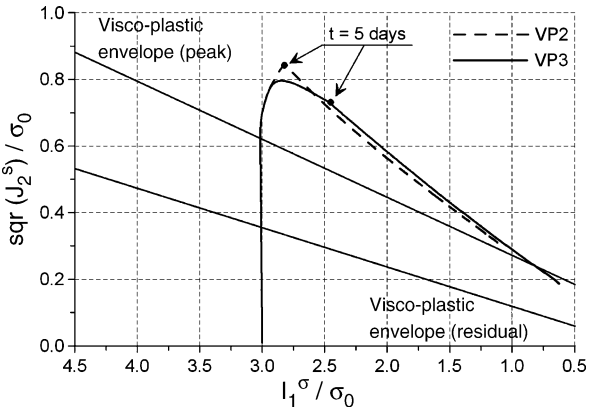

Fig. 11. Stress invariant path at the integration point closest to the tunnel crown for plane strain analyses with secondary (VP2) and tertiary (VP3) creep (I_1^σ = 1st invariant of the stress tensor, J_2^s = 2nd invariant of the deviatoric stress tensor, X_F = distance from the tunnel face)

enced by the heading effects. In the present context a length of 30 m was estimated, corresponding to approximately 3 times the tunnel diameter. Considering an advancing rate of 6 m/day, the plane strain calculation corresponds to a time span of 5 days.

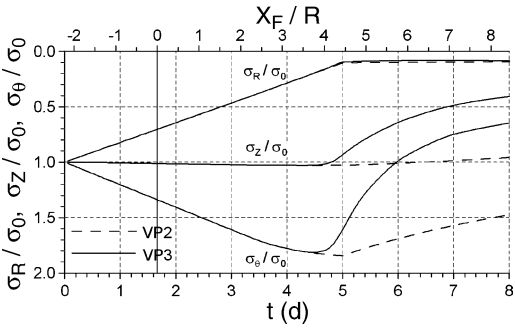

Fig. 12. Variation of principal radial σ_R, circumferential σ_θ and longitudinal σ_Z stresses with time and with distance X_F from the tunnel face, at the integration point closest to the tunnel crown, for plane strain analyses with secondary (VP2) and tertiary (VP3) creep (R = tunnel radius)

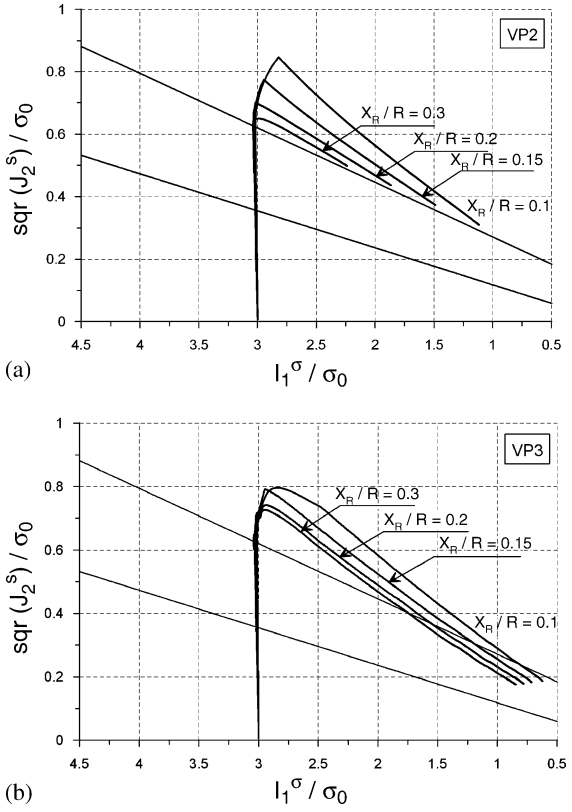

Fig. 13. Stress invariant paths at points at increasing distance X_R from the tunnel crown in the radial direction, for plane strain analyses with secondary (a) and tertiary (b) creep (I_1^σ = 1st invariant of the stress tensor, J_2^s = 2nd invariant of the deviatoric stress tensor, R = tunnel radius)

The results of the plane strain analyses are summarized in Figs. 10–13. Comparing the convergence diagrams in Fig. 10 with those in Fig. 6, for the axisymmetric case, it can be observed that the plane strain scheme does not provide accurate results in the vicinity of the excavation face. On the contrary, the long term closure, far away from the face, practically coincides in the two cases.

The stress invariant path (Fig. 11) for a point of the rock mass close to the tunnel contour, and the variation of the stress components during time (Fig. 12), are markedly different from those derived from the axisymmetric calculations. In particular, the increase of the first stress invariant is now absent (cf. Figs. 11 and 7) and no sharp variation of the stress components takes place at the tunnel face (cf. Figs. 12 and 8). Also in this case tertiary creep has a minor influence on the radial stress component.

Figure 13a, b refer, respectively, to the VP2 and VP3 plane strain analyses. They show the stress invariant paths of points at increasing distance X_R from the tunnel contour. Beside the difference with the axisymmetric results, it turns out that also in this case tertiary creep has a minor effect on the evolution of the invariants.

The distance X_F from the tunnel face in Fig. 13 was derived assuming that the heading influence covers a zone of 10 m (approximately one tunnel diameter) ahead of the face and of 20 m behind it.

The comparison between time dependent axisymmetric and plane strain results indicates that the latter scheme does not lead to an adequate prediction of convergence and stresses in the vicinity of the tunnel face. This represents a substantial drawback for the numerical analyses carried out during design and suggests using the axisymmetric scheme to this purpose.

6. Conclusions

A finite element study, based on axisymmetric and plane strain finite element analyses, has been presented on the effects of the time-dependent behaviour of rock on advancing tunnel.

The constitutive behaviour of the rock mass is described through a rheological model able to reproduce the three stage creep, namely: the visco-elastic (primary) creep, the visco-plastic (secondary) creep and the effects of tertiary creep, which is responsible of the squeezing conditions.

The model has been calibrated with reference to the intact rock behaviour, on the basis of laboratory creep tests presented in the literature. The parameters associated with the in situ rock mass have been derived from those of the intact rock adopting empirical relationships that depend on a measure of the rock mass conditions.

The numerical results of the tunnel problem have been discussed focusing especially on the influence of the excavation advancing on the tunnel closure and on the stress redistribution around it.

A first comment concerns both the importance and the difficulty of an accurate calibration of the rheological model. Since in situ creep tests are seldom performed, and the interpretation of data from monitored works is often difficult, empirical rules were adopted to scale the results of laboratory creep tests to the parameters of the rock mass. These correlations are based on rock quality indexes derived from borings or from geological observations.

It should be recognized, however, that the definition of such empirical relations for the creep behaviour is still an open issue and that the uncertainties inherent to the creep parameters of the rock mass may reflect on the results of the numerical analysis.

As expected, the finite element results show that the contribution of tertiary creep is crucial in the prediction of the short term closure of the tunnel. This could have a notable negative effect in case of TBM driven tunnels. In fact, even a relatively small convergence could lead to a rapid increase of the rock pressure on the shield that, in turn, could prevent the advancing of the machine.

The short term effect of the excavation advancing (i.e. in the vicinity of the tunnel face) seems properly described by the axisymmetric analyses, even though these are restricted to the case of hydrostatic and constant distribution of initial stresses.

The plane strain scheme, on the contrary, does not provide adequate results, in particular with respect to the tunnel convergence close to its heading. This is due to its intrinsic approximation introduced in the reduction of the rock pressure on the opening contour.

This suggests using an axisymmetric scheme, instead of the more popular plane strain one, for the evaluation of the short term effects in the presence of time dependent behaviour of rock.

Acknowledgments

The study is part of the National Research Project "Mechanized Tunnelling" (2001), coordinated by G. Barla and financially supported by the Italian Ministry of Education, University and Research.

List of Symbols

In this paper bold letters represent vectors, subscript s refers to the in situ conditions and the following symbols are used:

B^{el}	elastic bulk modulus;
c	cohesion associated with the yield function;
c_{lim}	cohesion associated with the visco-plastic envelope;
$\mathbf{e}$	deviatoric strain vector;
$\mathbf{e}^{el}$	deviatoric elastic strain vector;
$\mathbf{e}^{ve}$	deviatoric visco-elastic strain vector;
$\mathbf{e}^{vp}$	deviatoric visco-plastic strain vector;
$F(\boldsymbol{\sigma})$	yield function;
$F^{ve}(\boldsymbol{\sigma})$	visco-elastic envelope function;
$F^{vp}(\boldsymbol{\sigma})$	visco-plastic envelope function;
G^{el}	elastic tangential modulus;
G^{ve}	visco-elastic tangential modulus;
$I_1^{\boldsymbol{\sigma}}$	first invariant of the stress tensor;
J_2^{e-vp}	second invariant of the deviatoric visco-plastic strain tensor;
J_2^{s}	second invariant of the deviatoric stress tensor;
$Q(\boldsymbol{\sigma})$	visco-plastic potential function;
R_{CS}	ratio between σ_{lim} and σ_c;
R	tunnel radius;
$\mathbf{s}$	deviatoric stress vector;
t	time;
u	tunnel convergence;
X_F	distance from the tunnel face;
X_R	distance from the tunnel boundary in the radial direction;
$\boldsymbol{\varepsilon}$	total strain vector;

ε_v volumetric strain;
$\boldsymbol{\varepsilon}^{el}$ elastic strain vector;
$\boldsymbol{\varepsilon}^{ve}$ visco-elastic strain vector;
$\boldsymbol{\varepsilon}^{vp}$ visco-plastic strain vector;
ϕ friction angle associated with the yield function;
ϕ_{lim} friction angle associated with the visco-plastic envelope;
λ visco-plastic multiplier;
η^{ve} viscosity coefficient for visco-elasticity;
η^{vp} viscosity coefficient for visco-plasticity;
$\boldsymbol{\sigma}$ stress vector;
σ_0 initial, isotropic state of stress in the tunnel problem;
σ_c unconfined compression strength;
σ_{lim} maximum uniaxial compression stress at the visco-plastic limit condition;
σ_m hydrostatic stress;
$\boldsymbol{\sigma}^{vp}$ stress vector at the visco-plastic limit condition;
ψ_{lim} dilatancy associated with the visco-plastic envelope.

References

Aydan, Ö., Akagi, T., Kawamoto, T. (1996): The squeezing potential of rock around tunnels: theory and prediction with examples taken from Japan. Rock Mech. Rock Eng. 29, 125–143.

Barla, G. (1995): Squeezing rocks in tunnels. ISRM News J. II(3–4), 44–49.

Barla, G. (2002): Tunnelling under squeezing rock conditions. In: Kolymbas, D. (ed.), Eurosummer-School in Tunnel Mechanics, Innsbruck 2001, State of the art paper. Logos Verlag (Berlin) 169–268.

Barton, N. (2002): Some new Q-value correlations to assist in site characterisation and tunnel design. Int. J. Rock Mech. Min. 39(2), 185–216.

Boidy, E., Bouvard, A., Pellet, F. (2002): Back-analysis of time-dependent behaviour of a test gallery in claystone. Tunn. Undergr. Sp. Tech. 17, 415–424.

Chin, H. P., Rogers, J. D. (1987): Creep parameters of rocks on an engineering scale. Rock Mech. Rock Eng. 20, 137–146.

Cristescu, N. D., Gioda, G. (eds.) (1994): Visco-plastic behaviour of geomaterials. CISM Courses and Lectures n. 350, Springer-Verlag.

Cristescu, N. D., Hunsche, U. (1998): Time effects in rock mechanics, Wiley & Sons.

Dalgiç, S. (2002): Tunneling in squeezing rock, the Bolu tunnel, Anatolian Motorway, Turkey. Eng. Geol. 67, 73–96.

Dusseault, M. B., Fordham, C. J. (1993): Time-dependent behaviour of rocks. In: Hudson, J. A. (ed.), Comprehensive rock engineering, Vol. 3. Pergamon Press, 119–149.

Eberhardt, E. (2001): Numerical modelling of three-dimension stress rotation ahead of an advancing tunnel face. Int. J. Rock Mech. Min. Sci. 38, 499–518.

Einstein, H. H., Bobet, A. (1997): Mechanized tunnelling in squeezing rock – From basic thoughts to continuous tunnelling. In: Golser, J., Hinkel, W. J., Schubert, W. (eds.), Tunnels for people, Proc. 23rd ITA assembly, Wien Balkema, 619–632.

Gioda, G., Cividini, A. (1996): Numerical methods for the analysis of tunnel performance in squeezing rocks. Rock Mech. Rock Eng. 29(4), 171–193.

Hendron, A. J. (1968): Mechanical properties of rock. In: Stagg, K. G., Zienkiewicz, O. C. (eds.), Rock Mech. Eng. practice, Ch. 2, Wiley & Sons, 21–53.

Hoek, E. (1990): Estimating Mohr-Coulomb friction and cohesion values from the Hoek-Brown failure criterion. Int. J. Rock Mech. Min. Sci. 27(3), 227–229.

Hoek, E. (2001): Big tunnels in bad rock (36th Terzaghi Lecture). Int. J. Geotech. Geoenv. Engng. ASCE 127(9), 726–740.

Hoek, E., Brown, E. T. (1988): The Hoek-Brown failure criterion – a 1988 update. In: Curran, J. H. (ed.), Rock engineering for underground excavations, Proc. 15th Can. Rock Mech. Symp., Toronto Dept. Civil Engineering, University of Toronto, 31–38.

Hoek, E., Brown, E. T. (1997): Practical estimates of rock mass strength. Int. J. Rock Mech. Min. Sci. 34(8), 1165–1186.

Hoek, E., Diederichs, M. S. (2006): Empirical estimation of rock mass modulus. Int. J. Rock Mech. Min. Sci. 43(2), 203–215.

Kielbassa, S., Duddeck, H. (1991): Stress-strain fields at the tunnelling face – Three-dimensional analysis for two dimensional technical approach. Rock Mech. Rock Eng. 24, 115–132.

Kolymbas, D., Fellin, W., Kirsch, A. (2006): Squeezing due to stress relaxation in foliated rock. Int. J. Numer. Anal. Meth. Geomech. 30, 1357–1367.

Ladanyi, B. (1993): Time-dependent response of rock around tunnels. In: Hudson, J. A. (ed.), Comprehensive rock engineering, Vol. 2. Pergamon Press, 78–112.

Malan, D. F. (2002): Simulating the time-dependent behaviour of excavations in hard rock. Rock Mech. Rock Eng. 35(4), 225–254.

Panet, M. et al. (2001): Recommendations on the convergence-confinement method. AFTES Report, Version 1.

Pellet, F., Hajdu, A., Deleruyelle, F., Besnus, F. (2005): A visco-plastic model including anisotropic damage for the time dependent behaviour of rock. Int. J. Numer. Anal. Meth. Geomech. 29, 941–970.

Rivista Italiana di Geotecnica (Italian Geotechnical Journal) (2000): Special issue on squeezing rock conditions in tunnelling, Anno 34(1).

Rock Mechanics and Rock Engineering (1996): Special issues on tunnelling in squeezing rock, 29(3), 29(4).

Serafim, J. L., Pereira, J. P. (1983): Consideration of the geomechanical classification of Bieniawski, Proc. Int. Symp. Engineering geology and underground construction, Lisbon, Balkema 1, 33–44.

Shalabi, F. I. (2005): FE analysis of time-dependent behavior of tunneling in squeezing ground using two different creep models. Tunn. Undergr. Sp. Tech. 20, 271–279.

Singh, B., Goel, R. K., Jethwa, J. L., Dube, A. K. (1997): Support pressure assessment in arched underground openings through poor rock masses. Eng. Geol. 48, 59–81.

Starfield, A. M., McClain, W. C. (1973): Project Salt Vault: a case study in rock mechanics. Int. J. Rock Mech. Min. Sci. 10, 641–657.

Steiner, W. (1996): Tunnelling in squeezing rocks: case histories. Rock Mech. Rock Eng. 29, 211–246.

Thury, M., Bossart, P. (1999): The Mont Terri rock laboratory, a new international research project in a Mesozoic shale formation, in Switzerland. Eng. Geol. 52, 347–359.

Appendix

Equations (12) can be worked out combining, first, Eq. (4b) written for a biaxial state of stress,

$$\sigma_1^{\mathrm{vp}} + 2\sigma_2^{\mathrm{vp}} = \sigma_1 + 2\sigma_2, \tag{A1}$$

and Eq. (4c) with reference to a visco-plastic limit condition of Mohr-Coulomb type,

$$\sigma_1^{vp} = \sigma_2^{vp}\frac{1 + \sin\phi_{lim}}{1 - \sin\phi_{lim}} + \frac{2c_{lim}\cos\phi_{lim}}{1 - \sin\phi_{lim}}, \tag{A2}$$

to get the total stress carried by the plastic slider,

$$\sigma_1^{vp} = (\sigma_1 + 2\sigma_2)\frac{1 + \sin\phi_{lim}}{3 - \sin\phi_{lim}} + \frac{4c_{lim}\cos\phi_{lim}}{3 - \sin\phi_{lim}}, \tag{A3}$$

$$\sigma_2^{vp} = (\sigma_1 + 2\sigma_2)\frac{1 - \sin\phi_{lim}}{3 - \sin\phi_{lim}} - \frac{2c_{lim}\cos\phi_{lim}}{3 - \sin\phi_{lim}}. \tag{A4}$$

Then, the deviatoric stress carried by the dashpot is readily obtained by substituting the expressions (A3) and (A4) into Eq. (4a),

$$s_1^{vp} = \frac{2}{3 - \sin\phi_{lim}}[\sigma_1(1 - \sin\phi_{lim}) - \sigma_2(1 + \sin\phi_{lim}) - 2c_{lim}\cos\phi_{lim}], \tag{A5}$$

$$s_2^{vp} = -\frac{1}{3 - \sin\phi_{lim}}[\sigma_1(1 - \sin\phi_{lim}) - \sigma_2(1 + \sin\phi_{lim}) - 2c_{lim}\cos\phi_{lim}]. \tag{A6}$$

Considering the constitutive relationship of the dashpot, the deviatoric visco-plastic strain rates read:

$$\dot{e}_1^{vp} = \frac{2}{\eta^{vp}(3 - \sin\phi_{lim})}[\sigma_1(1 - \sin\phi_{lim}) - \sigma_2(1 + \sin\phi_{lim}) - 2c_{lim}\cos\phi_{lim}], \tag{A8}$$

$$\dot{e}_2^{vp} = -\frac{1}{\eta^{vp}(3 - \sin\phi_{lim})}[\sigma_1(1 - \sin\phi_{lim}) - \sigma_2(1 + \sin\phi_{lim}) - 2c_{lim}\cos\phi_{lim}]. \tag{A9}$$

Assuming a visco-plastic potential function Q^{vp} of Mohr-Coulomb type,

$$\sigma_1(1 - \sin\psi) - \sigma_2(1 + \sin\psi) - 2c^*\cos\psi = 0, \tag{A10}$$

the rate of the visco-plastic multiplier can be worked out from the expression (7) as follows:

$$\dot{\lambda} = \frac{(\dot{e}_1^{vp})^2 + 2(\dot{e}_2^{vp})^2}{\dot{e}_1^{vp}(1 - \sin\psi) - 2\dot{e}_2^{vp}(1 + \sin\psi)}. \tag{A11}$$

Substituting Eqs. (A8) and (A9) into Eq. (A11), and taking into account the flow rule (5), the rate of visco-plastic total strains in Eqs. (12) is finally reached,

$$\dot{\lambda} = \frac{3}{2\eta^{vp}(3 - \sin\phi_{lim})}[\sigma_1(1 - \sin\phi_{lim}) - \sigma_2(1 + \sin\phi_{lim}) - 2c_{lim}\cos\phi_{lim}]. \tag{A12}$$

Author's address: Donatella Sterpi, Department of Structural Engineering, Politecnico di Milano, P. Leonardo da Vinci 32, 20133 Milan, Italy; e-mail: sterpi@stru.polimi.it